Journal of Materials Chemistry

Cite this: *J. Mater. Chem.*, 2011, **21**, 9532

www.rsc.org/materials

PAPER

Highly defective MgO nanosheets from colloidal self-assembly†

Ben M. Maoz,[a] Einat Tirosh,[a] Maya Bar Sadan,[b] Inna Popov,[c] Yuri Rosenberg[d] and Gil Markovich*[a]

Received 12th January 2011, Accepted 4th May 2011
DOI: 10.1039/c1jm10181a

Highly defective magnesium oxide nanosheets were synthesized using a colloidal synthesis in which magnesium ethoxide was thermally decomposed in high-boiling-point weakly coordinating solvents. The nanosheets were assembled of small nanocrystal building blocks by oriented attachment. This assembly could be inhibited by using a strongly coordinating surfactant, such as oleic acid. The 2–3 nm spaced extended defects formed at the grain boundaries make up a material with a record defect density which causes an increased conductivity and dielectric constant, strong luminescence and paramagnetism. The point defect type prevailing at those interfaces is apparently charged oxygen vacancies. *In situ* TEM annealing experiments showed that the extended defects begin to anneal out at temperatures as low as 300 °C, but a high density of point defects apparently survives even at 750 °C.

Introduction

The ability to design and produce nanomaterials with new physical properties is a major goal in nanotechnology. Controlling the meso- and macroscopic structures of such materials, as in thin films, is also important for practical applications. Only recently it was shown that anisotropic assembly of nanoscale building blocks (BBs) is an important aspect in the generation of lower symmetry nanostructures of advanced materials.[1,2] Methods to control anisotropy in three dimensions are beginning to be realized, especially in superlattice structures,[3–5] and in particular, in pioneering work on two dimensional oriented attachment.[1–3,6] Yet, the concept of anisotropy is still largely underdeveloped in most particle assembly schemes.[7] The control of the oriented attachment of nanocrystalline BBs would allow production of relatively complex nanostructures and development of solution based techniques for the preparation of thin films. Some theoretical models describing oriented assembly were presented[6,8] but without a clear experimental proof of the anisotropic assembly mechanism. The assembly of very small BBs into much larger objects would result in a very large interfacial area which is prone to high defect concentrations. While defects are a nuisance in many materials applications, other functions, such as catalysis,[9,10] are enhanced by defects. They could also lead to unexpected phenomena, like inducing ferromagnetism in insulators with closed electronic shells.[11–13] Colloidal synthesis methods can produce defect concentrations that are far above those that could be found at equilibrium[13] due to the relatively low temperature limit of the organic solvents involved (350–400 °C). In contrast to the successes in the preparation of size controlled colloidal transition metal-oxide nanocrystals,[14–19] colloidal alkaline earth oxide nanocrystals are particularly difficult to produce by wet colloidal techniques. This difficulty arises from their tendency to form hydroxides and carbonates. Only recently a first publication on the synthesis of colloidal nanocrystalline MgO has appeared.[20]

In the present work we describe a new colloidal synthesis of MgO by thermal decomposition of Mg-ethoxide in high boiling point solvents (such as oleylamine and trioctylphosphine oxide) under a nitrogen atmosphere. MgO nanosheets (NSs) were formed by spontaneous oriented assembly of very small MgO nanocrystal BBs where the interfaces between the BBs formed a very high density of defects. These defects were found to induce strong luminescence, strong paramagnetism, and relatively high conductivity and dielectric constant at the NSs. The magnetic properties of the NSs were recently published elsewhere.[21]

Experimental

The MgO-NSs were synthesized under a nitrogen atmosphere in two steps: first, the preparation of the precursor, magnesium ethoxide ($Mg(OCH_2CH_3)_2$), and then its thermal decomposition in a high boiling point coordinating solvent to form the MgO nanocrystals. It is possible to synthesize MgO from commercially available magnesium alkoxides. This was avoided due to the presence of transition metal impurities at the >10 ppm level in these materials. Thus, ultra-pure Mg (99.998%) was chosen as the starting point for the synthesis.

[a]*School of Chemistry, Tel Aviv University, Tel Aviv, 69978, Israel. E-mail: gilmar@post.tau.ac.il*
[b]*Institute of Solid State Research, Ernst Ruska-Centre for Microscopy and Spectroscopy with Electrons—Research Centre Jülich GmbH, D-52425 Jülich, Germany*
[c]*The Center for Nanoscience and Nanotechnology, Hebrew University, Jerusalem, 91904, Israel*
[d]*The Wolfson Applied Materials Research Center, Tel Aviv University, Tel Aviv, 69978, Israel*

† Electronic supplementary information (ESI) available: Nitrogen adsorption isotherm, additional TEM images, XPS results and thermogravimetric analysis. See DOI: 10.1039/c1jm10181a

Preparation of ultrapure Mg-ethoxide

4.0 g (164 mmol) of distilled Mg, dendritic pieces, 99.998% pure (Sigma-Aldrich), were added to 200 mL (3.43 mol) of anhydrous ethanol (Gadot lab supplies) under a nitrogen environment. The reaction mixture was heated to 40 °C and vigorously stirred for 3 h until a white $Mg(OH)_2$ precipitate was formed. This stage was essential in order to completely dry the ethanol. The ethanol was then filtered and added to a flask with the Mg pieces, and the reaction mixture was stirred vigorously and heated to reflux for 48 h under nitrogen flow. The ethanol mixture was evaporated in vacuum at ≤40 °C, until a white precipitate was formed. The $Mg(OCH_2CH_3)_2$ was identified by NMR and IR spectroscopies.

MgO NS synthesis

500 mg (329 mmol) of $Mg(OCH_2CH_3)_2$ were added to 40 mL (3.43 mol) oleylamine (Sigma-Aldrich) and the reaction mixture was stirred vigorously and heated to boiling at about 338 °C for 2 h under a nitrogen flow. The MgO-NSs were also prepared in other coordinating solvents (trioctylamine, trioctylphosphine oxide) using the exact same method described above and exhibited the same results. After the solution was cooled to room temperature, a mixture of acetone and ethanol (1 : 1) was added to the oleylamine solution to precipitate the NSs and they were separated out by centrifugation at 6000 rpm for 6 min. The precipitate was re-dissolved in heptane. Then, again, a mixture of acetone and ethanol was added to the solution to precipitate the NSs to wash excess oleylamine, followed by centrifugation and evaporation of the remaining heptane to obtain purified MgO NSs, with a yield of ~80%. All these steps were done under a nitrogen atmosphere.

MgO nanocrystal synthesis

About 200 mmol oleic acid was added to the solution of the Mg $(OCH_2CH_3)_2$. The rest of the process was identical to the NS preparation.

Preparation of MgO control sample

Mg chips, 4–30 mesh, 99.98% (Sigma-Aldrich), were burned in air, at ~3000 °C, and the resulting MgO nanoparticle smoke was directly sampled on TEM grids.

Characterization

The NSs were characterized by a Tecnai F20 HR-TEM.

X-Ray diffraction (XRD) data were collected with Cu Kα radiation on a Θ–Θ "Scintag" powder diffractometer equipped with a liquid nitrogen cooled Ge solid-state detector. XRD patterns were treated by JADE 9.1+ software (JADE 9.1+ software, Materials Data Inc., Livermore, CA, 94550, USA) including a whole pattern fitting (WPF)/Rietveld refinement.

Measurements of the complex dielectric constant were done on a Novocontrol broadband dielectric spectrometer BDS 80, based on an Alpha High Resolution Dielectric Analyzer (NOVOCONTROL) and an automatic Quatro temperature control system. MgO NS powder pellets were made as follows: gold was evaporated on polished 1″ stainless steel discs. In the nitrogen filled glove box, the MgO NS's powder was pressed between two such discs coated with a gold film.

EPR measurements were collected by a Bruker ELEXYS 500 (X band at 9.5 GHz) spectrometer. The powder was put in quartz tubes (Suprasil, Wilmad-Labglass).

Results and discussion

The MgO-NSs were assembled two-dimensionally from 3–5 nm nanocrystal BBs with lateral dimensions of ~100 to 1000 nm, and about single nanocrystal thick (see Fig. 1). The NS powder had a specific surface area of about 250 $m^2\ g^{-1}$ (Fig. S1†). When oleic acid surfactant molecules were added to the reaction mixture they prevented the formation of NSs and isolated 10–40 nm single crystal nanoparticles (NPs) were produced (Fig. 2b).

Simulations of the assembly of ionic CdTe nanocrystals were able to describe such anisotropic assembly processes when competing Coulomb, dispersion and dipole–dipole interactions were included.[6,8] Both CdTe and MgO are cubic crystals with a high degree of symmetry, thus the mechanism suggested in these simulations may be applicable to MgO BB assembly.

The main parameters that affected the MgO-NSs formation are the heating rate and the type of solvent/surfactant used. The ratio of MgO to $Mg(OH)_2$ was estimated by a whole pattern fitting of the XRD data. It was found that reducing the heating rate down to 10 °C min^{-1} resulted in an increasing amount of $Mg(OH)_2$ in the sample (see Table 1) while a fast heating rate of 30 °C min^{-1} produced MgO exclusively. The slow heating slowed down the MgO nucleation which probably occurred at a higher temperature than the hydroxide formation and thus led to an increasing probability of reaction with residual water to form the hydroxide.

This is probably due to the limited time for residual water molecules to react with the Mg-ethoxide precursor relative to the faster precursor decomposition rate to MgO and ethanol, which occurs at higher temperatures.

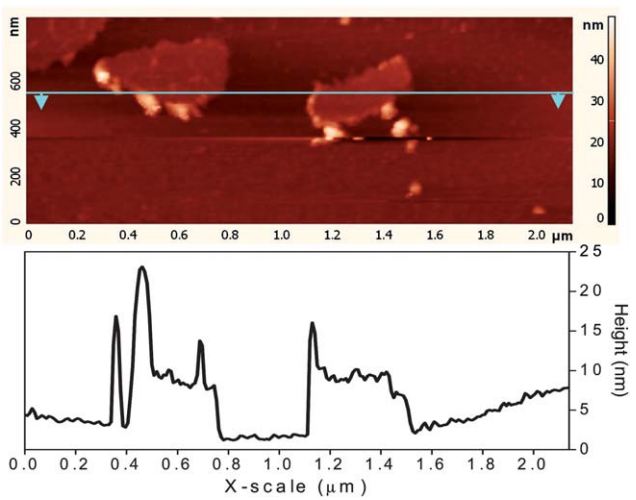

Fig. 1 An AFM topography image of two NSs deposited on a silicon wafer, with a corresponding height profile along the line marked on the image. A sheet thickness of about 6–7 nm is visible, which is probably the thickness of the MgO NSs + the oleylamine surfactant layer.

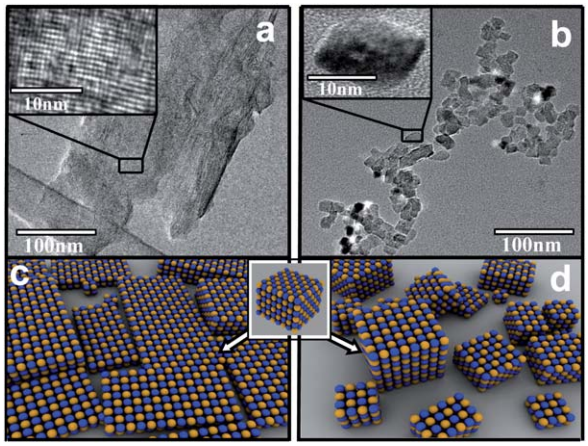

Fig. 2 (a) TEM image of an MgO NS laying over a hole in a carbon support film. (b) MgO nanocrystals grown with oleic acid. (c) An illustration of the NS assembly from BB's. (d) An illustration of the isolated nanocrystals grown out of BBs.

Table 1 Product composition *vs.* heating rate as estimated by whole XRD pattern fitting

Heating rate/°C min^{-1}	Product composition (%) MgO : $Mg(OH)_2$
30	100 : 0
20	75 : 25
15	50 : 50
10	0 : 100

A possible MgO nanocrystal BB formation mechanism is related to the cubane structure found for Mg-methoxide, where the material forms $(Mg–O–CH_3)_4$ cubic units.[22] The structure of Mg-ethoxide used in the present work is expected to be similar to the structure of the Mg-methoxide. Thus, the precursor probably maintains the cores' $(Mg–O–)_4$ cubane structure at the relatively low synthesis temperature (~300 °C). The MgO-NSs were obtained in both non-coordinating and weakly coordinating solvents, which indicates, that the solvent does not play a significant role, as long as it does not bind strongly to the oxide surface as in the oleic acid case.

The XRD patterns of the as-prepared and annealed at 750 °C powder samples are shown in Fig. 3a, where the as prepared pattern is up-shifted for clarity. The annealing caused essential narrowing of the Bragg diffraction peaks and their shift to larger angles, indicating a lattice parameter decrease.

The detailed annealing temperature dependence of the MgO lattice parameter and the size of coherent scattering domain (CSD—"grain" or crystallite size) determined by a whole pattern fitting procedure are shown in Fig. 3b. The major increase in CSD size, from ~3 nm for the as-prepared up to ~30 nm, was obtained on heating at 750 °C, reflecting the onset of a sintering process. A possible cause for the increased lattice parameter in the as prepared NSs could be a high concentration of point defects, such as vacancies or interstitial atoms, like hydrogen, which would correspond to hydroxyl groups trapped within the lattice.[23] The Fourier-filtered HR-TEM image in Fig. 4a reveals that the NSs are highly defective. Analysis of HR-TEM images

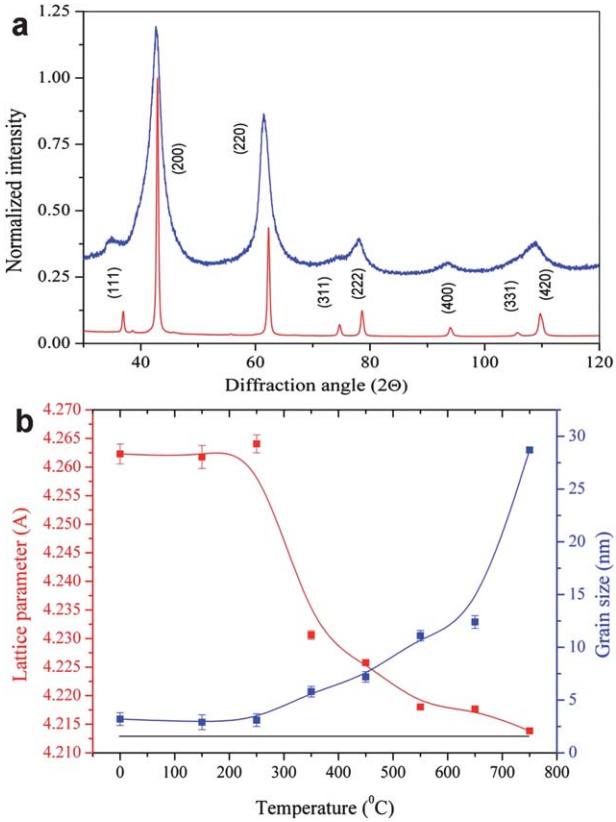

Fig. 3 X-Ray diffraction analysis of MgO-NSs. (a) XRD patterns of the as-synthesized (top curve) and annealed at 750 °C (bottom curve) MgO-NSs. (b) Red curve—lattice parameter of MgO *vs.* annealing temperature. Blue curve—CSD size (calculated from XRD line-widths) *vs.* annealing temperature. The horizontal line at the bottom is the bulk lattice parameter.

of many NSs showed that the NSs always have one of the principle axes of the cubic crystal perpendicular to their plane (see Fig. 5). The dislocations appear along the principal axes of the crystal, with an average separation between them of about 2 nm, which corresponds to a dislocation density of about 10^{13} cm^{-2}. This is one of the highest defect densities that were measured and close to the theoretical limit of dislocation density.[24] This value correlates well with the ~3 nm CSD for the same sample by XRD. Thus, we conclude that both techniques indicate that the as synthesized material is composed of about 2–3 nm crystallites of MgO.

As seen in Fig. 3, the gradual growth of crystallite size started at about 300 °C, which is the temperature at which the lattice parameter begins to decrease, nearly approaching the bulk value of 4.211 Å at 750 °C. To further study the low temperature annealing process, the MgO-NSs were heated in high vacuum using a TEM heating holder. This *in situ* heating experiment enabled us to gradually change the dislocation density and to track the changes in defect density in the NSs. A Fourier filtered lattice image of a NS taken at ~300 °C (Fig. 4b) displays a higher degree of ordering relative to the as-prepared NS of Fig. 4a. The Fourier transform of the HR-TEM image shown in the inset of Fig. 4a indicates that the as-prepared NSs maintain a long range orientational order, along a common [100] axis although with some local misorientation. The Fourier transform of the *in situ*

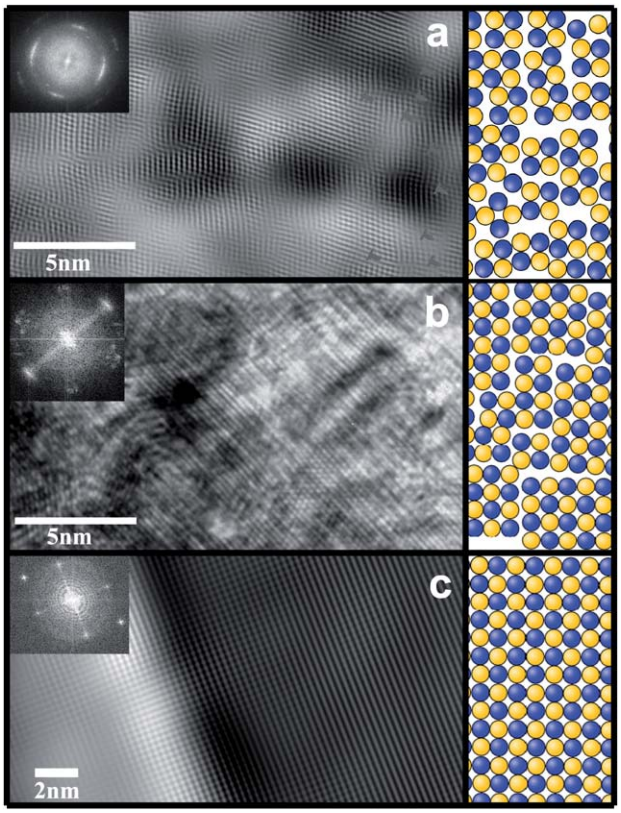

Fig. 4 (a) Fourier-filtered HR TEM images of an as-prepared NS. Numerous dislocations are clearly visible. Some of them are marked by arrows for clarity. The Fourier transformed image at the inset confirms a common, although not perfect, orientation over the whole observed NS. (b) A NS under *in situ* heating in the TEM at ~300 °C. The lower quality of the figure is due to the shorter exposure time imposed by the thermal drifts inherent in such experiments. The Fourier transformed image at the inset indicates a higher degree of order of nanodomains toward a single crystalline structure, although structural defects are still visible in the lattice image. (c) The reference MgO (high temperature combustion). The Fourier transformed image at the inset exhibits a well-defined single crystal pattern.

heated NS (Fig. 4b) looks closer to a zone axis pattern of a perfect single crystal (as the inset in Fig. 4c) than to a textured pattern of a polycrystalline material (as the inset in Fig. 4a). The remarkably low annealing temperature observed in this experiment demonstrates the metastable nature of these highly defective NSs.

The observed dislocations in the NSs are believed to originate in the grain boundaries defined by the BB assembly process. To further analyze the mechanism leading to this assembly, one should bear in mind that the MgO has a highly ionic character and that the solvent has a low dielectric constant. Rough calculations show that one excess negative ion on one [100] face and one positive ion on the opposite face over a 3 nm wide MgO BB would yield a dipole moment of ~140 D. Due to the low dielectric medium there should be a relatively strong long range dipole–dipole interaction to guide the assembly of the BBs. Moreover, when the BBs get closer to a separation smaller than their own size (~1 nm or below), specific local interactions probably dominate the oriented attachment (Fig. 5). Since the BBs are presumably produced with random surface defects, there will be some anisotropy in the charge distribution around the BBs, as well as around the growing sheet, even at [100] type surfaces which are supposed to have charge neutral planes, as seen in Fig. 5. This should produce substantial dipole moments as well as higher multipoles at the particles. The BB–NS dipolar interaction may then favor attachment in the plane of the sheet rather than on top, in particular if there is also some net charging of the BBs and NSs,[25] which is reasonable to expect. These results are consistent with both experimental,[26–28] and theoretical[29] studies, which show a preference for alignment of MgO nanocrystallites with commensurate [100] surface.

The addition of a strongly binding surfactant, such as oleic acid, prevents the NS assembly by keeping the separation between the BBs and only allows for further growth of the BBs as isolated nanocrystals.

Fig. 6 displays temperature dependent complex AC permittivity data measured on the as-prepared NS powder at a frequency of 1 Hz. The imaginary component is proportional to the conductivity of the material. The high dielectric constant and conductivity indicate a strongly thermally activated charge mobility, which reaches a maximal conductivity of $\sim 6 \times 10^{-9}$ S m^{-1} at 470 K which is almost 3 orders of magnitude greater than the bulk value.[30,31] The dielectric constant was about 30 times

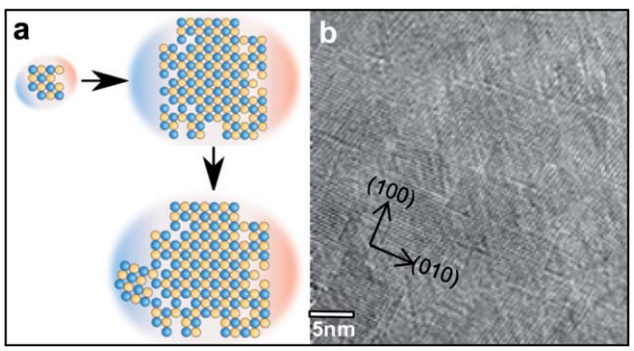

Fig. 5 (a) An illustration of the assembly mechanism, showing the dipole moments developed in the MgO nanostructures due to surface defects. (b) A spherical aberration corrected HR-TEM image of an as-prepared NS.

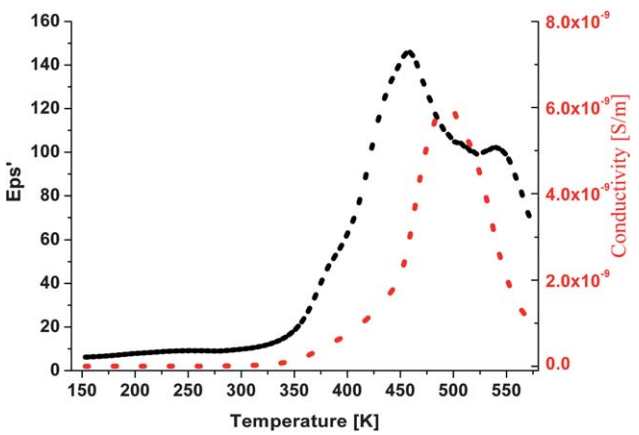

Fig. 6 Complex dielectric constant measurement of the as-prepared NS powder at 1 Hz *vs.* temperature. The conductivity is proportional to the imaginary component of the dielectric constant.

higher than the bulk value.[32] A relatively low charge delocalization energy barrier of ~300 meV was estimated from an Arrhenius fit of the temperature dependence of the conductivity peak frequency. We note that this result matches the energy barrier estimated by McKenna and Shluger for valence band holes trapped at dislocations or grain boundaries.[33]

Point defects in insulators such as MgO may form luminescent centers in the material. Fig. 7a shows 3 powder samples, (1) the as prepared NSs, (2) a NS powder annealed at 300 °C, and (3) the control MgO sample prepared by burning Mg in air. Fig. 7b shows their blue/UV luminescence upon excitation by an ultraviolet lamp at ~330 nm, demonstrating that the as-prepared sample is highly photoluminescent relative to the control sample, and also more luminescent relative to the annealed sample. Fig. 7c shows the emission spectrum of the as-prepared NSs dispersed in chloroform, when excited at a wavelength of 337 nm. Identification of the source of defect luminescence in MgO is a complex problem which is yet to be resolved. A broad emission similar to the ~400 nm emission band of the NS sample was previously observed by Moon *et al.* in colloidal nanocrystals and attributed to surface defects.[20] Knozinger and coworkers have observed photoluminescence in CVD grown MgO,[28] which was slightly blue shifted relative to the present work, with emission maxima at 365–375 nm, but at much shorter excitation wavelengths (<270 nm). This luminescence was associated with excitations of low-coordination oxygen surface sites. According to calculations by McKenna and Shluger the origin of the emission band of the NSs could be the excitation of valence electrons to half-filled surface (grain boundary) F^+ states, namely, unpaired electrons trapped in an oxygen vacancy.[33]

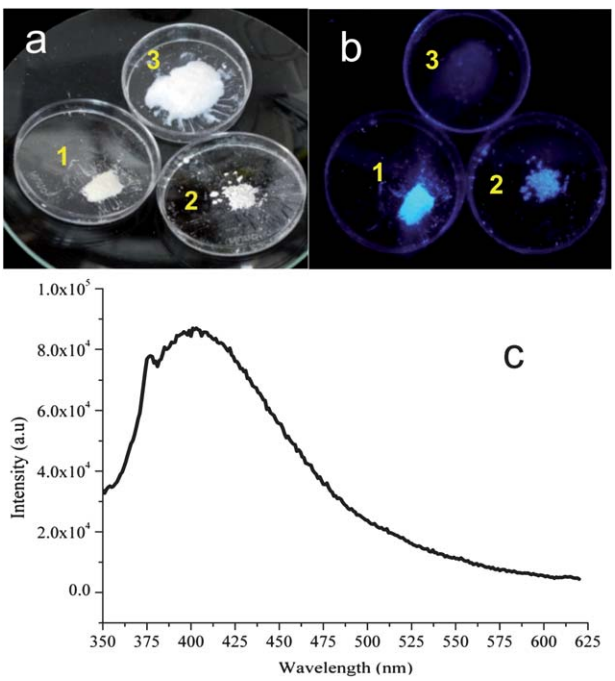

Fig. 7 (a) Three NS powder samples: (1) as-prepared NSs, (2) annealed at 300 °C, and (3) MgO control sample. (b) Visible photoluminescence of the three samples on excitation with a UV lamp at ~330 nm. (c) The emission spectrum of the NSs dispersed in chloroform. Excitation wavelength was 337 nm.

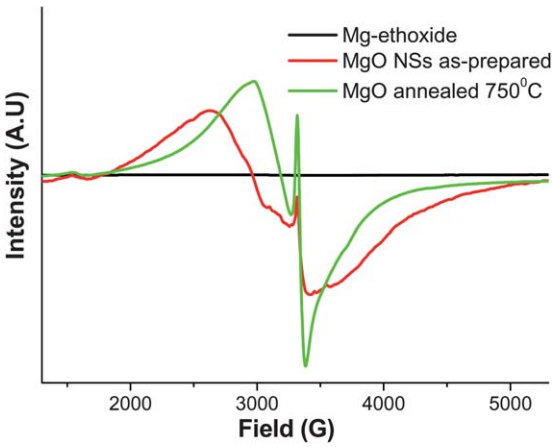

Fig. 8 Room temperature X-band EPR spectra of three samples.

XPS measurements (Fig. S3†) of the 1s binding energy of Mg detected a binding energy increase of more than 1.4 eV between the as-prepared and the annealed sample. This shift in the binding energy indicates that the Mg in the as-prepared sample is not fully oxidized and implies that the sample is dominated by oxygen vacancies. After the sample was annealed in air, oxygen atoms filled some of the vacancies and fully oxidized the Mg.

Another important characterization tool of the defects is EPR spectroscopy. The EPR data in Fig. 8 do not resemble any previous EPR measurements of point defects in bulk-like MgO.[34] The as-prepared NS sample exhibits a strong paramagnetic signal mainly consisting of a strongly shifted signal towards low resonance field values, which indicates that the defect spins were strongly interacting. The precursor material, Mg-ethoxide, showed negligible paramagnetic signal. The annealed sample had more weakly interacting spins with a larger fraction of non-interacting spins at $g \approx 2$. These results conform with the conductivity results, where spin–spin interactions and relatively high conductivity characterize the as-prepared sample, and when annealed, the inter-defect interaction is significantly reduced.

Consequently, combining the XPS, photoluminescence, EPR results and theoretical calculation data[33] it is believed that the prevailing type of point defects is dense, interfacial oxygen vacancies of F^+ type carrying a magnetic moment. While structural changes begin to show around 300 °C, the high point defect density seems to survive even after annealing at 750 °C, as seen in the EPR data.

Conclusions

In summary, this work describes a colloidal MgO synthesis producing one of the most defective MgO, with a high surface area to volume ratio. The NS assembly mechanism described in this work is supported by recent theoretical work, where a combination of BB dipole moments, charging and short-range dispersion interactions was responsible for the 2D BB assembly. The strong ionic character of MgO leads to the generation of large BB dipole/multipole moments by random surface defects.

The physical properties of the NSs are rather unique, including strong luminescence, enhanced dielectric constant, relatively high conductivity, strong inter-defect magnetic coupling and high

surface to volume ratio. These properties conform with the recent finding of low-temperature ferromagnetism in the MgO NSs.[21]

The ability to exploit the anisotropic assembly of the ionic BBs is of practical importance as a low cost method to fabricate two dimensional structures that may go hand in hand with the conventional thin film deposition methods. We believe that the new type of MgO nanomaterial described here will be useful for catalysis applications, where the high surface area and surface defects play a crucial role,[9,10] and will help resolving fundamental questions about the theoretical defect density limit, and the repulsion energy of neighboring dislocation.

Acknowledgements

This research was supported by The Israel Science Foundation grant no. 779/06. The authors are grateful to Denis Glozman for the drawings, Dr Lothar Houben and Dr Yossi Lereah for fruitful discussions, and to Dr Lev Wiener, Dr Larisa Burstein, Dr Anna Greenbaum, and Prof. Dina Goldnitsky for their help with the various characterizations.

Notes and references

1 C. Schliehe, B. H. Juarez, M. Pelletier, S. Jander, D. Greshnykh, M. Nagel, A. Meyer, S. Foerster, A. Kornowski, C. Klinke and H. Weller, *Science*, 2010, **329**, 550.
2 Z. Tang, Z. Zhang, Y. Wang, S. C. Glotzer and N. A. Kotov, *Science*, 2006, **314**, 274.
3 M. R. Jones, R. J. Macfarlane, B. Lee, J. Zhang, K. L. Young, A. J. Senesi and C. A. Mirkin, *Nat. Mater.*, 2010, **9**, 913.
4 E. V. Shevchenko, D. V. Talapin, N. A. Kotov, S. O'Brien and C. B. Murray, *Nature*, 2006, **439**, 55.
5 D. V. Talapin, E. V. Shevchenko, C. B. Murray, A. V. Titov and P. Kral, *Nano Lett.*, 2007, **7**, 1213.
6 Z. Zhang, Z. Tang, N. A. Kotov and S. C. Glotzer, *Nano Lett.*, 2007, **7**, 1670.
7 S. C. Glotzer and M. J. Solomon, *Nat. Mater.*, 2007, **6**, 557.
8 S. Shanbhag and N. A. Kotov, *J. Phys. Chem. B*, 2006, **110**, 12211.
9 B. Yoon, H. Hakkinen, U. Landman, A. S. Worz, J. M. Antonietti, S. Abbet, K. Judai and U. Heiz, *Science*, 2005, **307**, 403–407.
10 G. Pacchioni, J. M. Ricart and F. Illas, *J. Am. Chem. Soc.*, 1994, **116**, 10152–10158.
11 A. Droghetti, C. D. Pemmaraju and S. Sanvito, *Phys. Rev. B: Condens. Matter Mater. Phys.*, 2010, **81**, 092403.
12 I. Elfimov, S. S. Yunoki and G. A. Sawatzky, *Phys. Rev. Lett.*, 2002, **89**, 216403.
13 E. Tirosh and G. Markovich, *Adv. Mater.*, 2007, **19**, 2608.
14 N. R. Jana, Y. Chen and X. Peng, *Chem. Mater.*, 2004, **16**, 3931.
15 M. Niederberger, M. H. Bartl and G. D. Stucky, *Chem. Mater.*, 2002, **14**, 4364.
16 M. Niederberger, G. Garnweitner, N. Pinna and G. Neri, *Prog. Solid State Chem.*, 2005, **33**, 59.
17 J. Park, K. An, Y. Hwang, J. G. Park, H. J. Noh, J. Y. Kim, J. H. Park, N. M. Hwang and T. Hyeon, *Nat. Mater.*, 2004, **3**, 891.
18 S. Sun, H. Zeng, D. B. Robinson, S. Raoux, P. M. Rice, S. X. Wang and G. Li, *J. Am. Chem. Soc.*, 2004, **126**, 273.
19 J. Tang, J. Fabbri, R. D. Robinson, Y. Zhu, I. P. Herman, M. L. Steigerwald and L. E. Brus, *Chem. Mater.*, 2004, **16**, 1336.
20 H. R. Moon, J. J. Urban and J. D. Milliron, *Angew. Chem., Int. Ed.*, 2009, **48**, 6278.
21 B. M. Maoz, E. Tirosh, M. Bar Sadan and G. Markovich, *Phys. Rev. B: Condens. Matter Mater. Phys.*, 2011, **83**, 161201(R).
22 S. Wuttke, A. Lehmann, G. Scholz, M. Feist, A. Dimitrov, S. I. Troyanov and E. Kemnitz, *Dalton Trans.*, 2009, 4729–4734.
23 A. Cimino, P. Porta and M. Valigi, *J. Am. Ceram. Soc.*, 1966, **49**, 152.
24 R. M. J. Cotterill, *Phys. Lett. A*, 1977, **60**, 61.
25 C. Noguera and G. Jacek, *J. Phys.: Condens. Matter*, 2008, **20**, 264003.
26 P. Chaudhari and J. W. Matthews, *J. Appl. Phys.*, 1971, **42**, 3063.
27 A. Moses-Ezhil-Raj, L. C. Nehru, M. Jayachandran and C. Sanjeeviraja, *Cryst. Res. Technol.*, 2007, **42**, 867.
28 S. Stankic, J. Bernardi, O. Diwald and E. Knozinger, *J. Phys. Chem. B*, 2006, **110**, 13866.
29 K. P. McKenna, P. V. Sushko and A. L. Shluger, *J. Am. Chem. Soc.*, 2007, **129**, 8600.
30 S. P. Mitoff, *J. Chem. Phys.*, 1959, **31**, 1261.
31 E. Yamaka and K. Sawamoto, *J. Phys. Soc. Jpn.*, 1955, **10**, 176.
32 X.-S. Fang, C.-H. Ye, T. Xie, Z. Y. Wang, J. W. Zhao and L. D. Zhang, *Appl. Phys. Lett.*, 2006, **88**, 013101.
33 K. P. McKenna and A. L. Shluger, *Phys. Rev. B: Condens. Matter Mater. Phys.*, 2009, **79**, 224116.
34 M. Chiesa, E. Giamello and M. Che, *Chem. Rev.*, 2010, **110**, 1320.